Journal of Structural Geology, Vol. 15, Nos 3–5, pp. 403 to 411, 1993
Printed in Great Britain

0191-8141/93 $06.00+0.00

The analysis of progressive deformation in rock analogues

PAUL D. BONS*

Institute of Earth Sciences, Utrecht University, P.O. Box 80.021, 3508 TA Utrecht, The Netherlands

MARK W. JESSELL

Victorian Institute of Earth and Planetary Sciences, Department of Earth Sciences, Monash University, Clayton, Melbourne, Victoria 3168, Australia

and

CEES W. PASSCHIER

Institute of Earth Sciences, Utrecht University, P.O. Box 80.021, 3508 TA Utrecht, The Netherlands

(*Received* 16 *December* 1991; *accepted in revised form* 6 *July* 1992)

Abstract—Two-dimensional deformation experiments using analogue materials such as octachloropropane and camphor have proven to be a powerful tool in the investigation of microstructural development, since they make it possible to observe the specimen throughout its deformation history. The addition of dispersed marker particles makes it possible to trace the movement of material points during deformation. From this information the flow and deformation can be interpolated for any point within the specimen at any time. The geometry of the flow and deformation can then be visualized in the form of grids, contour-plots, strain ellipses and other methods.

Despite this apparently ideal setting for studying flow and deformation, the need to use marker particles to trace material points introduces unexpected problems in the analysis. We present a computer program to analyse the movement of marker particles. Digitization of the positions of the particles is improved by the use of video input and semi-automatic digitization. The use of polynomials to describe the complete path of marker particles and least-squares best-fit solving improves the analysis of the data.

INTRODUCTION

THE development of microstructures during ductile deformation in rocks can be modelled with crystalline rock analogues such as octachloropropane and camphor that exhibit crystal-plastic behaviour at room temperature. These materials can be deformed between thin glass plates in a rig that can be mounted on a microscope stage (Means 1977, 1989 and references therein). In this way a deforming specimen can be observed throughout its deformation history. Analogue experiments are becoming increasingly popular for research and teaching purposes because they are the only technique available to structural geologists in which the processes and kinematics of deformation can be directly observed at the grain scale. They are useful tools for demonstrating the principles of recrystallization, twinning and shear zone development.

One of the main aims of analogue experiments is the determination of the kinematics of deformation, which can then be linked to the observed microstructural phenomena. Progressive deformation can be studied by tracking the relative displacements of material points. It is not practical to inscribe a grid on the thin specimens of, for example, camphor as is the practice with clay or wax experiments (e.g. Mancktelow 1991) and grain boundaries cannot serve as marker particles since they migrate through the material (e.g. Urai *et al.* 1986). Therefore small opaque marker particles are dispersed through the material (grinding power (SiC), ≈5–30 μm in size). These particles move passively along with the deforming material (Means 1980, Jessell 1986).

Micrographs or video-images can be taken at specific intervals during an experiment. This produces a series of images with dispersed dots (Fig. 1). Two steps have to be taken from this stage to produce, for instance, plots showing the distribution of finite strain for a deformation episode between two photographs:

(1) digitization of the positions of each marker at each recorded stage;

(2) actual analysis of the kinematics of deformation.

The first step can be rather difficult if performed manually. Marker particles have to be as small as possible in order not to influence the experiment, and therefore recognition of individual marker particles is difficult. Pattern recognition is therefore used to identify individual marker particles from a recognizable group.

The second step is analogous to the analysis of deformation using an inscribed grid (e.g. Mancktelow 1991). A difference is that our marker particles are randomly

* Present address: Victorian Institute of Earth and Planetary Sciences, Department of Earth Sciences, Monash University, Clayton, Melbourne, Victoria 3168, Australia.

distributed. An imaginary grid has to be superposed on the specimen. For each grid node the deformation is then analysed using the displacements of the marker particles nearest to that node. A simple method for this is described by Jessell (1986). It is based on the principle that if the positions before and after deformation of three marker particles are known, the position gradient tensor can be exactly calculated if deformation was homogeneous in the triangle with the three marker particles at its corners. The minimum number of three marker particles is derived from the fact that a tensor can only be reconstructed if changes in position of at least two points with respect to a third point are known. A third point is the base of the reference frame in which the tensor description is calculated. This method, however, is very sensitive to inevitable errors in digitized marker-particle positions (ten Brink unpublished data). A more sophisticated approach is to use a least-squares approximation, which is less sensitive to these errors. It may also be desirable to know the material flow in the specimen rather than the finite deformation after a certain deformation increment. For this purpose velocities of marker particles have to be used instead of displacements.

In this paper we first discuss the basic principles of how to derive the position gradient tensor or velocity gradient tensor and then we present a number of ways to visualize the results. At the end we discuss one application of the method: investigation of grain-boundary migration. Illustrations are derived from a typical experiment with polycrystalline norcamphor ($C_7H_{10}O$), deformed under pure shear conditions at 45°C (≈0.85 homologous temperature) (Figs. 1, 3, 6 and 7).

We have developed a program that automates the major part of the marker-particle digitization and performs the deformation analysis (see Appendix). It is specifically designed to analyse finite deformation and flow using randomly distributed marker particles. The latter is however not a requirement and it can be used to analyse inscribed grids as well.

THE METHOD

Basic principles

In any deforming body, material will be moving with respect to an external reference frame. We need to distinguish between deformation, which is the field describing the finite changes in position of material points, and flow, which is the field describing the instantaneous velocities of these points. If the position of a material point after deformation $\mathbf{x}'$ (see Table 1 for list of symbols) is assumed to be a function of its original position ($\mathbf{x}$) (e.g. McKenzie 1979, Spencer 1980, Passchier 1988, Means 1990), then:

$$\mathbf{x}' = \mathbf{F}\mathbf{x} + \mathbf{d}, \tag{1}$$

with $\mathbf{F}$ being the position gradient tensor and $\mathbf{d}$ the rigid-body translation vector. The displacement vector $\Delta\mathbf{x}$ of a material point is a function of $\mathbf{x}$ as follows:

$$\Delta\mathbf{x} = \mathbf{x}' - \mathbf{x} = (\mathbf{F}-\mathbf{I})\mathbf{x} + \mathbf{d}, \tag{2}$$

where $\mathbf{I}$ is the identity-tensor. Deformation is homogeneous if $\mathbf{F}$ does not vary as a function of $\mathbf{x}$. If $\mathbf{v}$ is the velocity of a material point at position $\mathbf{x}$, the velocity gradient tensor ($\mathbf{L}$) and the rigid body velocity vector $\boldsymbol{l}$ can be defined in a similar way (Spencer 1980, Passchier 1987):

$$\mathbf{v} = \mathbf{L}\mathbf{x} + \boldsymbol{l}, \tag{3}$$

Again, if $\mathbf{L}$ does not vary as a function of $\mathbf{x}$, flow is homogeneous. In reality deformation or flow will rarely be homogeneous and the aim of the analysis is to find the distribution of $\mathbf{F}$, $\mathbf{d}$, $\mathbf{L}$ and $\boldsymbol{l}$ in the deforming material by solving equations (1)–(3).

The marker particles represent a set of material points of which the positions $\mathbf{x}$ are known at specific moments during progressive deformation when their positions were recorded on micrographs or on video (Fig. 2a). This is the basic set of data, which can be used to solve equations (1) or (2). The velocities of marker particles, needed to solve equation (3) are however not known, but they can be approximated in the following way. Assuming that the actual paths of the marker particles are smooth, the positions of these marker particles at any time t can be interpolated, by describing the position of each marker as a function of time:

$$\mathbf{x} = \mathbf{x}(t). \tag{4}$$

We have chosen a polynomial function (Fig. 2b), treating position in each direction ($i = 1,2$) separately:

$$x_i(t) = \sum_{n=0}^{N} (c_n)_i t^n. \tag{5}$$

The order N of the polynomials can be adjusted to the complexity of the paths and the number of time-increments recorded. The $N + 1$ coefficients $(c_n)_i$ in each polynomial can be calculated with a least-squares best-fit method. The advantage of using polynomials is that a limited set of coefficients defines the whole path for each marker particle. These coefficients can be calculated once and stored in memory or on file for later use. Another advantage of using a smoothed path to describe the positions of marker particles is that errors in digitizing the positions of marker particles can be smoothed, if a suitable order of the polynomial is chosen. Now that we have the position of each marker as a function of time, the velocity of each marker particle at any time can be calculated by taking the derivative with respect to time at the desired time,

$$v_i(t) = \sum_{n=1}^{N} (c_n)_i t^{n-1}. \tag{6}$$

To solve equation (2) (describing the deformation) one needs data on the position of marker particles at

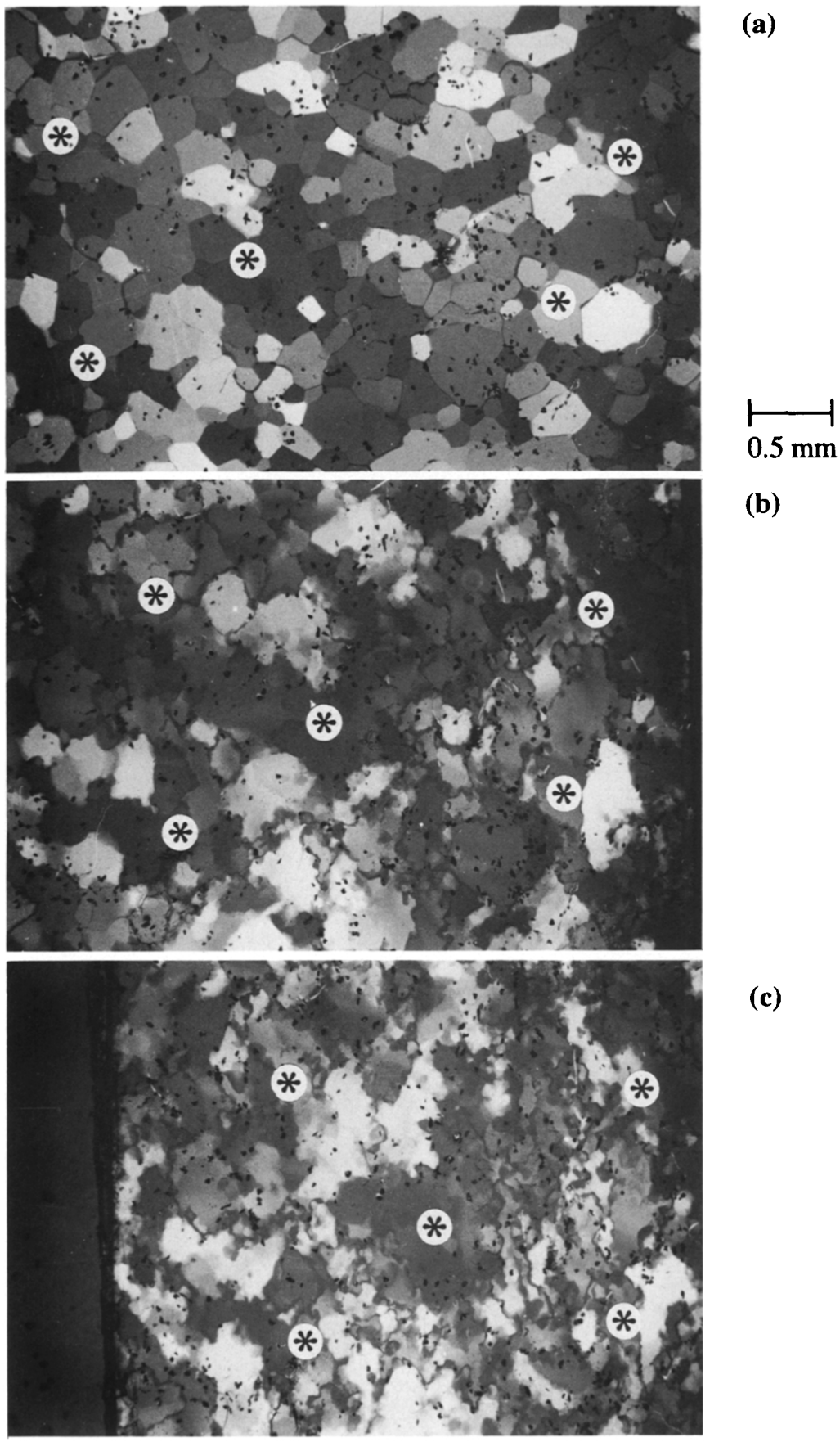

Fig 1. Micrographs of deforming norcamphor, taken at t = 0 (a), 33 (b) and 66 (c) min. Shortening is in the E–W direction. Scale bar is 0.5 mm. Small dots are SiC marker particles. The displacement of the marker particles can be used to determine deformation parameters. The five solid dots are marker particles that are also drawn on the plots in Figs. 6 and 7. Note the dynamic recrystallization, especially at the right, where strain localization occurs.

Table 1. List of symbols. Vector symbols are written in lower case bold and tensor symbols in upper case bold

x	Position vector of material point before deformation increment
x'	Position vector of material point after deformation increment
Δx	Displacement vector of a material point
v	Velocity vector of material point
F	Position gradient tensor
L	Velocity gradient tensor
I	Identity tensor or Kronecker delta δ_{ij}
d	Rigid-body translation vector
l	Rigid-body velocity vector
t	Time
c	Polynomial coefficient
N	Polynomial order
W	Vorticity (Means *et al.* 1980)
S	Spin
W_k	Kinematic vorticity number (Truesdell 1953)

two times. These can be the times of digitization, or any chosen times if marker particle paths are calculated with equation (5). To solve equation (3) (describing flow), the positions of marker particles at a certain time and their velocities have to be known. These data have to be derived from equations (5) and (6).

In the case of both deformation and flow, a set of vectors (**Δx** or **v**) at a set of points (**x**) are known. Using these data, equations (2) or (3) have to be solved for the whole area of interest. As these equations are essentially of the same form, the method is the same for both deformation and flow, and yields either **F** − **I** and **d**, or **L** and ***l***. These are calculated for regularly distributed points in the field of interest, for instance the nodes of a rectangular grid.

To solve equations (2) and (3) for a node, deformation has to be treated as having been homogeneous in a small area around that node so that small-scale inhomogeneities are neglected. These equations can then be solved exactly with three data points (marker particles) that lie in the area near the node. Using more data points over-determines the solution and a least-squares best-fit method has to be used. The advantage of the latter is that the effect of digitizing errors is subdued. The program therefore uses at least four data points, which have to be distributed around the node, to calculate **F** and **d** or **L** and ***l***, by solving equation (2) or (3). The maximum area for which deformation is treated as homogeneous is defined interactively by the user. If one uses all data points one gets the bulk **F** and **d**, or **L** and ***l*** (Mancktelow 1991) (Fig. 3).

If the area is too small, not enough data points will

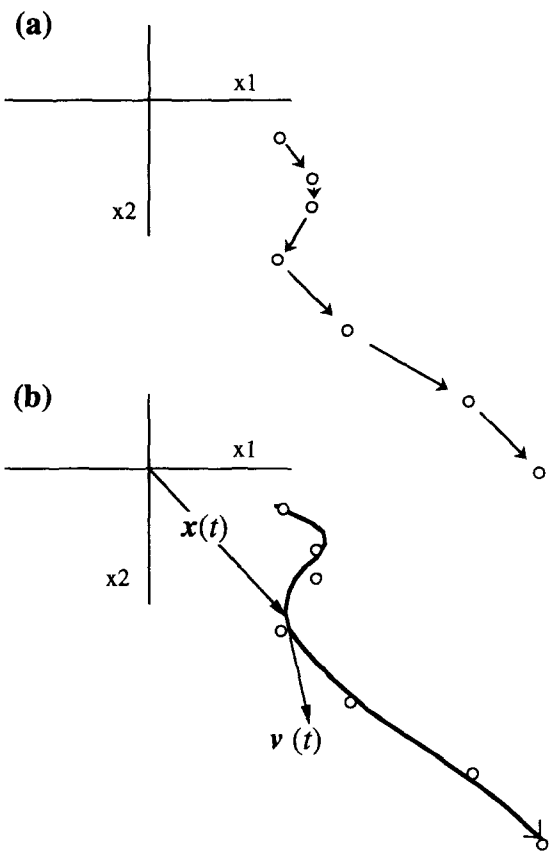

Fig. 2. The approximation of the path of a marker particle from measured positions (dots) at discrete intervals. (a) Position of the particle at seven times during the deformation. (b) Least-squares best-fit with a fourth-order polynomial in x_1 and x_2 directions separately, describing the position, **x**, as a function of time, *t*. It is possible to assign a velocity vector **v** to the marker-particle at any time. This velocity vector lies at a tangent to the inferred movement path.

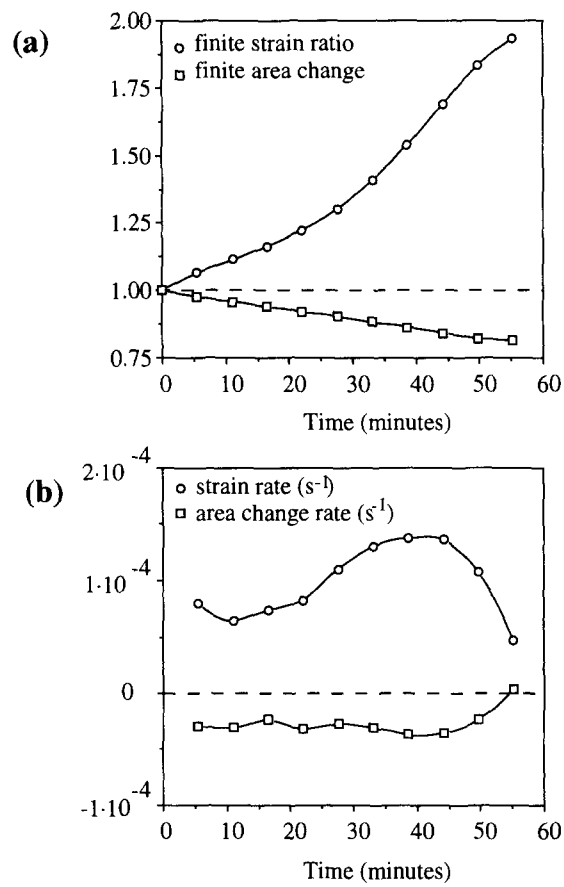

Fig. 3. Bulk flow and finite strain in the norcamphor experiment shown in Fig. 1, calculated by interpolating velocity and displacement vectors of all marker particles. The marker particles occupied a region of approximately 3.5 × 2.5 mm^2, which is about 10% of the whole area of the specimen. (a) Finite strain ratio and finite area change as a function of time. There is a significant loss in area (≈18%), probably caused by thickening of the specimen. (b) Strain rate and area change rate as a function of time. Note that the strain rate changes with time, because of strain localization either inside or outside the region occupied by the marker particles.

lie in the area and if the area is set too large, deformation cannot be treated as having been homogeneous and the method cannot be used. However, if these requirements are met, the program solves equation (2) or (3) and after all nodes have been dealt with, **F** and **d** or **L** and *l* are known for the nodes of the grid.

Error reduction

The resulting tensor and vector have certain errors, caused by: (1) errors in the digitized positions of marker particles or measurement-errors; and (2) heterogeneity of deformation around the grid node. The treatment of deformation in the area occupied by four marker particles as having been homogeneous is only approximately valid if this area is small (and thus the density of marker particles high) relative to the deformation gradient. However, when the marker-particle density is high, the errors in determining the marker positions become relatively more important. The density of marker particles should therefore be adjusted to the accuracy of measurement of their positions. In practice there will always be a certain error in the interpolated tensors and vectors. These errors will multiply when deformation-parameters are calculated from the tensors.

Data can be enhanced by using the fact that analogue experiments are carried out in thin samples between stiff glass plates and that the analogue materials are practically incompressible. This information is not used in the calculations described above. If the experiment is exactly plane-strain, the area change in the plane of measurement should always be zero. In most cases however the whole sample will flatten or thicken somewhat. Area change will vary gradually over the sample or even be constant. One can now iteratively adjust **d** or **v** of each grid node to fulfil the requirement of homogeneous area change for a small area around the grid node. Now **F** or **L** can be recalculated using **d** or **v** of the surrounding grid nodes. An example of the effect of this improvement is given in Fig. 4. One should note that this enhancement may only be carried out if there is reason to believe that area changes vary only gradually. When, for instance, grain-boundary diffusion or pressure solution are the deformation mechanisms, this is clearly not the case (Ree personal communication).

Vorticity and spin

A special problem in kinematic analysis is the distinction between vorticity (W) and spin (S) in progressive deformation (Fig. 5). Vorticity is defined as the summed angular velocity of orthogonal material lines with respect to the instantaneous stretching axes (ISA), while spin is the rotation of ISA in an external reference frame (Means *et al.* 1980, Lister & Williams 1983, Passchier 1986, 1987). From a position gradient tensor **F** representing a single deformation increment, it is possible to measure the rotation of two orthogonal

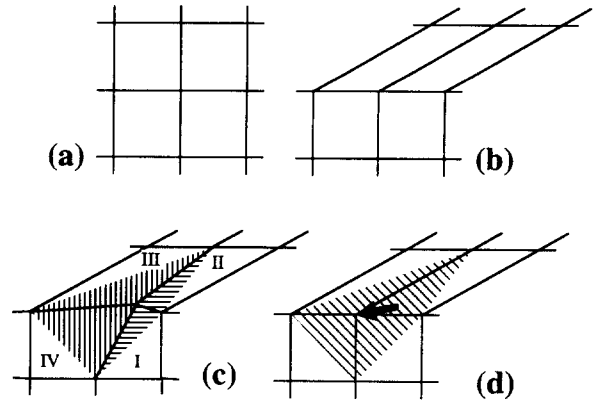

Fig. 4. The procedure to reposition grid nodes assuming incompressibility and using an initially square grid. (a) Actual situation before the strain increment. (b) Actual situation after the strain increment. (c) Interpolated grid with an obviously erroneous interpolation of the displacement of the middle grid node. Four neighbouring triangles are dashed according to their apparent area change: triangles I and II are too small, triangles III and IV too large. (d) The interpolated grid after repositioning (arrow) the middle grid node, in such a way that all four triangles have the same size.

material lines with respect to an external reference frame. A sum of mean vorticity and spin can be determined in this way if flow parameters do not change rapidly during the increment. To calculate mean spin, only the difference in orientation of ISA before and after the same deformation increment have to be measured. These can be derived from the velocity gradient tensors **L** at the beginning and at the end of the deformation increment. The method described in this paper allows for the calculation of both **F** and **L**, so in principle spin and vorticity can be distinguished. The procedure is as follows.

For a deformation increment from t_1 to t_2 at a certain point **x** (a grid node) one can calculate:

(a) the local velocity gradient tensor, $\mathbf{L}_{(t_1,\mathbf{x})}$, at that point from the velocity vectors of the surrounding marker particles at t_1;

(b) the local position gradient tensor, $\mathbf{F}_{(t_1-t_2,\mathbf{x})}$, at that point for the whole deformation increment, using the displacement vectors of the surrounding marker particles, which gives the position **x**′ of the material point **x** after the deformation increment; and

(c) the local velocity gradient tensor, $\mathbf{L}_{(t_2,\mathbf{x}')}$, at point **x**′ from the velocity vectors of the surrounding marker particles at t_2.

The ISA orientations at t_1 and t_2 are now known, and the orientation of the deformed material lines which were originally the ISA at t_1, can be calculated and compared with the principal stretching directions (PSD), which are the long and short axes of the strain ellipsoid. Figure 5 shows the results for four cases with time-independent deformation. In case of zero vorticity the PSD and the material lines which coincided with the ISA at t_1 should be identical at t_2. When vorticity is non-zero these two do not coincide.

Note that $\mathbf{L}_{(t_1,\mathbf{x})}$ and $\mathbf{L}_{(t_2,\mathbf{x}')}$ can only be calculated if the positions of marker particles were recorded at at least three stages of the deformation, and preferably more. If the positions are only known at two stages,

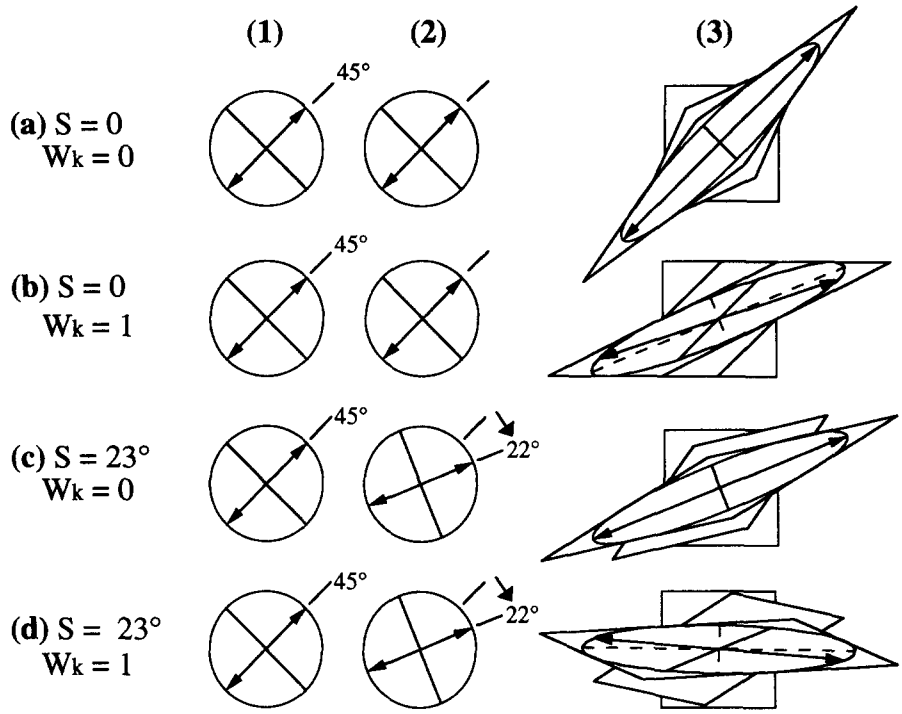

Fig. 5. The analysis of spin (S) and vorticity (given as kinematic vorticity number W_k) for four cases: (a) $S = 0°$ and $W_k = 0$. (b) $S = 0°$ and $W_k = 1$. (c) $S = 23°$ and $W_k = 0$. (d) $S = 23°$ and $W_k = 1$. Column (1) shows the orientation of the ISA before the strain increment ($t = t_1$), column (2) shows the same at the end of the strain increment ($t = t_2$). Column (3) shows the finite deformation and rotation of an original square. Finite strain ellipses are drawn in the deformed squares, with the principal stretching directions (PSD) as dashed lines and the material lines that coincided with the ISA of $t = t_0$ as solid lines.

$\mathbf{L}_{(t_1,\mathbf{x})}$ and $\mathbf{L}_{(t_2,\mathbf{x}')}$ will always be the same as both calculated velocity vectors and displacement vectors will lie parallel. An inherent problem of vorticity and spin analysis is that the deformation increment must be large to accurately determine $\mathbf{F}$, whereas it should be as small as possible to approximate time-independent flow parameters during the increment. This inevitably puts limitations on the accuracy of distinguishing between spin and vorticity.

Visualization

Once $\mathbf{F}$ and $\mathbf{d}$ or $\mathbf{L}$ and l are calculated for all grid nodes, several techniques that have been incorporated

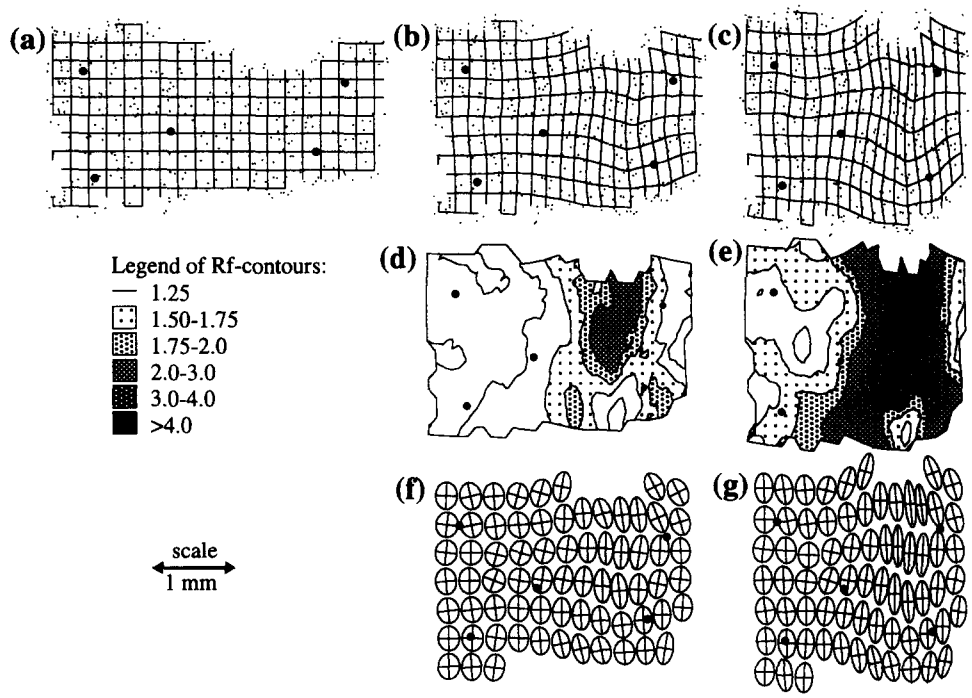

Fig. 6. Plots showing finite deformation parameters for the norcamphor experiment shown in Fig. 1. The five solid dots are the marker particles highlighted in Fig. 1. (a)–(c) Deformed grids at $t = 0$, 33 and 55 min. Small dots represent marker particles. (d) & (e) Finite strain ratio contours at $t = 33$ and 55 min. (f) & (g) Finite strain ellipses at $t = 33$ and 55 min.

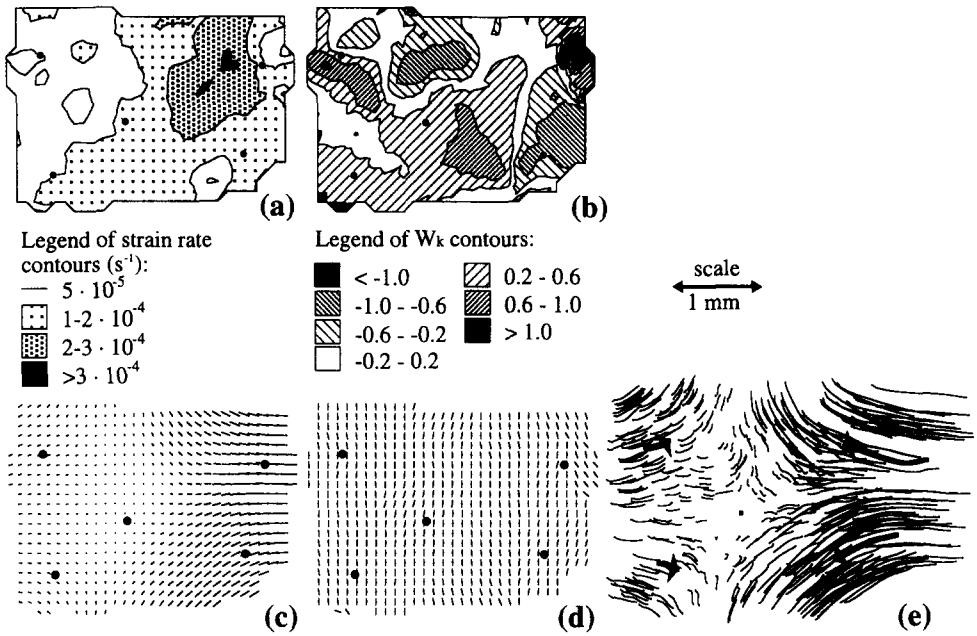

Fig. 7. Plots showing flow parameters for the norcamphor experiment shown in Fig. 1 at t = 33 min. The five solid dots are the marker particles highlighted in Fig. 1. (a) Contours of strain rate. (b) Contours of kinematic vorticity number W_k, uncorrected for spin. (c) Plot of velocity vectors. (d) Plot of ISA orientation. (e) Approximate paths of all markers from t = 0 to t = 55 min. The paths are approximated with fourth-order polynomials.

into the program can be used for displaying the deformation field. Examples are given in Figs. 6 and 7.

The first display mode is a 'deformed grid', which is probably the best way to visualize finite deformation (Figs. 6a–c). This grid is constructed by adding the displacement **d** of each grid node to its original position and linking all nodes with straight lines. A number of kinematic parameters such as vorticity and stretching rate can be calculated from the tensors **F** and **L** (Passchier 1988a, Means 1990) which are best displayed in the form of contour-plots (Figs. 6d & e and 7a & b). Strain ellipses show the magnitude of finite strain and the direction of the principal stretching directions (Figs. 6f & g). Plots of velocity vectors or displacement vectors demonstrate the flow pattern in the material (Fig. 7c). This can also be done by drawing the paths of all marker particles (Fig. 7e). It can also be useful to plot the orientations of ISA at a certain time (Fig. 7d). Plots of these orientations can be a tool to recognize inhomogeneities in vorticity and/or spin.

Grain-boundary migration

Analogue experiments are well suited to study grain-boundary migration (Jessell 1986, Urai *et al.* 1986, Wilson 1986, Urai 1987, Means & Ree 1988). During deformation grain boundaries will change their shape due to two different processes: (a) because grain boundaries move passively *with* the deforming material (strain); and (b) because they migrate *through* the material (grain-boundary migration). At first sight these two modes of shape change of grain boundaries are often indistinguishable. To determine actual amount of grain-boundary migration the following method can be used (Fig. 8).

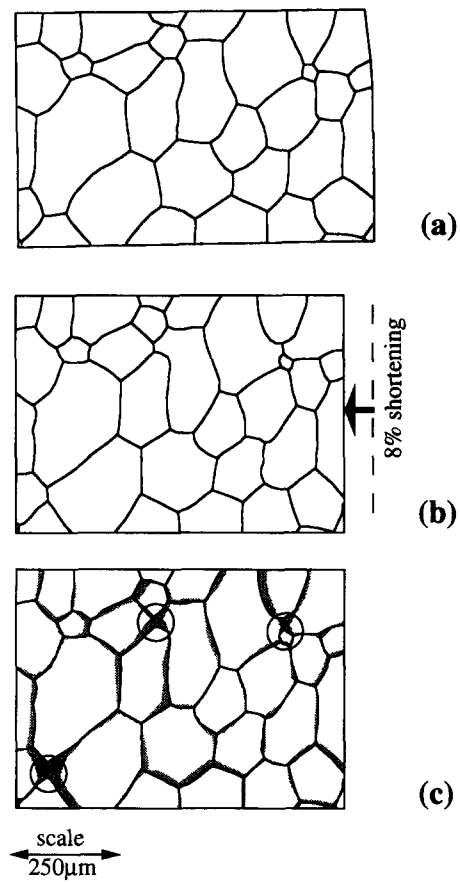

Fig. 8. Example of the analysis of grain-boundary migration, taken from an experiment with octachloropropane (C_3Cl_8), deformed under pure shear at an applied strain rate of 2×10^{-5} s^{-1} and a temperature of 75°C. (a) Digitized grain boundaries at beginning of strain increment (t = 0 min). (b) Digitized grain boundaries at t = 72 min after strain increment of about 8% shortening in an E–W direction. (c) Original grain boundaries (t = 0 min) are repositioned as passive markers, according to the deformation field calculated with the marker particles, and superposed on the actual grain boundaries at t = 72 min. The areas through which grain boundaries have migrated are shaded. Note three neighbour-switching events (circles).

Grain boundaries before and after a deformation increment are digitized in the form of points (nodes) linked by straight lines (Figs. 8a & b). Just as **F** and **d** could be calculated for nodes on a grid, they can be calculated for the nodes on grain boundaries. 'Deformed grain boundaries' can be constructed in the same way as a 'deformed grid'. The 'deformed grain boundaries' represent the grain boundaries after the deformation increment if no grain-boundary migration has taken place. The difference between the actual position of grain boundaries after deformation and the calculated 'deformed grain boundaries' represents the actual grain-boundary migration (shaded areas in Fig. 8c).

CONCLUSIONS

Although analogue experiments seem to produce an 'ideal' data set where 'everything is known', it is still surprisingly difficult to calculate some parameters of deformation and flow. This is due to the inherent problems in the determination of the instantaneous movement of particles, in the recognition of a material point and in the errors in determining its position. The method described here allows us to analyse such a data set and to extract as much information as possible. The use of functions describing positions of marker particles as a function of time, makes it possible to determine the flow field in the deforming material, instead of only the finite deformation.

Acknowledgements—We wish to thank Boudewijn van Milligen and Majid Hassanisadeh for their suggestions and for reviewing the principles of the method. Furthermore we thank Coen ten Brink, Win Means, Jin Han Ree, Janos Urai and the reviewers Stefan Schmid, Renée Heilbronner and an anonymous reviewer for criticism and suggestions. Paul Bons acknowledges the financial support by The Netherlands Organization for Scientific Research and the hospitality of the Department of Earth Sciences of Monash University, Melbourne, Australia.

REFERENCES

Jessell, M. W. 1986. Grain boundary migration and fabric development in experimentally deformed octachloropropane. *J. Struct. Geol.* **8**, 527–542.

Lister, G. S. & Williams, P. F. 1983. The partitioning of deformation in flowing rock masses. *Tectonophysics* **92**, 1–33.

Mancktelow, N. S. 1991. The analysis of progressive deformation from an inscribed grid. *J. Struct. Geol.* **13**, 859–864.

McKenzie, D. 1979. Finite deformation during fluid flow. *Geophys. J. R. astr. Soc.* **58**, 689–715.

Means, W. D. 1977. A deformation experiment in transmitted light. *Earth Planet. Sci. Lett.* **35**, 169–177.

Means, W. D. 1980. High temperature simple shearing fabrics: a new experimental approach. *J. Struct. Geol.* **2**, 197–202.

Means, W. D. 1989. Synkinematic microscopy of transparent polycrystals. *J. Struct. Geol.* **11**, 163–174.

Means. W. D. 1990. Kinematics, stress, deformation, and material behaviour. *J. Struct. Geol.* **12**, 953–971.

Means, W. D., Hobbs, B. E., Lister, G. S. & Williams, P. F. 1980. Vorticity and non-coaxiality in progressive deformations. *J. Struct. Geol.* **2**, 371–378.

Means, W. D. & Ree, J. H. 1988. Seven types of subgrain boundaries in octachloropropane. *J. Struct. Geol.* **10**, 765–770.

Passchier, C. W. 1986. Flow in natural shear zones—the consequences of spinning flow regimes. *Earth Planet. Sci. Lett.* **77**, 70–80.

Passchier, C. W. 1987. Efficient use of the velocity gradients tensor in flow modelling. *Tectonophysics* **136**, 159–163.

Passchier, C. W. 1988. Analysis of deformation paths in shear zones. *Geol. Rdsch.* **77**, 309–318.

Spencer, A. J. M. 1980. *Continuum Mechanics*. Longman, London.

Truesdell, C. 1953. Two measures of vorticity. *J. Rational Mech. Anal.* **2**, 173–217.

Urai, J. L. 1987. Development of microstructure during deformation of carnallite and bischofite in transmitted light. *Tectonophysics* **135**, 251–263.

Urai, J. L., Means, W. D. & Lister, G. S. 1986. Dynamic recrystallization of minerals. *Am. Geophys. Un. Geophys Monogr.* **36**, 161–199.

Wilson, C. J. L. 1986. Deformation induced recrystallization of ice: the application of in situ experiments. *Am. Geophys. Un. Geophys. Monogr.* **36**, 213–232.

APPENDIX

Computer program

All routines described in this paper are combined into two compatible and fully menu-driven programs, implemented for Apple Macintosh computers. The programs are written in C. Full colour screen and about 1 Mb of RAM are recommended. All output is in TEXT- or PICT-format which is compatible with most graphics-, spreadsheet- and word-processing applications available for Apple Macintosh computers. The program occupies 214 kb and can be obtained free from the authors. Please include a 3.5″ floppy disk. A manual is in preparation.